Estimates of mode-1 internal tide harmonic generation in the global ocean

Scott Wunsch◉ and F. Joseph Marcellino ◉*

The Johns Hopkins University Applied Physics Laboratory, Laurel, Maryland 20723, USA

Recent theoretical and experimental work has demonstrated the generation of nonlinear harmonics when internal waves propagate in nonuniform stratification. This effect is most pronounced if the harmonic frequency is near resonance with a freely propagating mode. It may play a significant role in the evolution of low-mode internal tides in the ocean, possibly leading to the formation of strongly nonlinear waves. Here, global ocean stratification profiles measured by ARGO floats are used to quantify the potential for nonlinear harmonic generation for semidiurnal mode-1 internal tides. The results show that the first harmonic, with double the wave number of the parent mode, is often expected to attain an amplitude exceeding a fifth of the parent mode in equatorial regions. Potentially strong harmonic responses were calculated most frequently for the Pacific and Indian Oceans. A strong harmonic is not expected in the Atlantic, despite near-resonance conditions, because weaker and more shallow pycnoclines do not provide a sufficient harmonic forcing. Hence near resonance is found to be a necessary, but not sufficient, condition for harmonic generation in measured ocean stratifications. A second criterion, based on pycnocline depth and density change, is proposed as an additional condition for harmonic generation.

I. INTRODUCTION

Recent work has shown that internal waves propagating through nonuniform stratification generate double-frequency and double-wave-number harmonics. This effect has been demonstrated for internal waves incident on a pycnocline in both the laboratory [1–3] and in numerical simulations [4–6]. The harmonic effect was first shown theoretically for a sharp interface by Thorpe [7] and was generalized to any nonuniform stratification profile using weakly nonlinear theory in [5]. This work also demonstrated that the amplitude of the harmonic mode would be greatest in instances of near resonance, in which the harmonic frequency was nearly equal to the frequency of a freely propagating wave with the harmonic wave number. The harmonic mode arises due to self-interaction of the parent internal wave with itself in regions where the density gradient is changing and is a special case of resonant triads in nonuniform stratifications [8].

The weakly nonlinear theory of harmonic generation has recently been applied to mode-1 internal tides in [9–13]. Mooring data from the South China Sea [14] has indicated the intermittent presence of a double-frequency harmonic of the diurnal tide which could be associated with this effect. Motivated by these observations, the authors of Ref. [9] used idealized ocean stratification profiles based on MOODS data [15] to estimate the steady-state amplitude of the harmonic that would theoretically be generated by the semidiurnal (mode-1) internal tide. The results suggested that the harmonic mode could plausibly generate near surface currents with amplitudes on the order of 0.1 m/s, a value roughly consistent with the South China Sea observations of [14]. (However, mere consistency is not proof that this is the mechanism responsible for the observations, given the

---

*Present address: University of Geneva, 1205 Geneva, Switzerland.

124801-1

complicated environment found there.) Subsequent numerical simulations [10] with an idealized ocean stratification profile also demonstrated the formation of the double-frequency harmonic mode. In [11], the weakly nonlinear theory of [5] was extended to include rotation and the initial growth dynamics of the mode-1 internal tide. Analytic results for idealized ocean stratification profiles indicated that significant harmonic generation was expected due to near resonance of the primary and harmonic modes in the absence of rotation but that increasing rotation would break this resonance and prevent the growth of the harmonic mode. This suggested that the harmonic generation mechanism was most likely to occur in equatorial oceans (latitudes less than ∼20 degrees). The timescale for growth of the harmonic mode was found to be on the order of a few days, also consistent with the observations of [14].

In [12], the weakly nonlinear theory of [11] was extended to couple the parent and harmonic mode amplitudes and better represent the dynamics of near-resonant harmonics using a separation of timescales approach. It was shown that a steady-state harmonic amplitude does not generally occur, but instead the parent and harmonic modes slowly oscillate in amplitude as they exchange energy, reminiscent of the intermittent harmonics seen in the South China Sea data of [14]. The accuracy of the weakly nonlinear theory was verified using numerical simulations. For idealized ocean profiles in equatorial regions, the improved theory also indicated harmonic mode growth timescales of a few days. The theoretical approach was further extended in [13] to include higher harmonics, which could yield a transition to a strongly nonlinear solitary internal wave.

In the global ocean, the mode-1 semidiurnal internal tides have been observed to contain ∼36 pJ of energy, based on satellite observations [16]. Given the recent theoretical understanding of nonlinear harmonic generation and the importance of mode-1 ocean internal tides, the present work uses measured ARGO [17] stratification profiles to calculate the expected characteristics of the mode-1 harmonic in the global ocean. Existing theory is applied for this purpose, with the caveat that many important aspects of ocean dynamics (such as ocean currents and horizontal variations in stratification and bathymetry along the propagation path) are neglected. The goal of this analysis is to determine if realistic ocean stratification profiles could potentially yield nonlinear harmonic generation. The results support the previously published speculation, which was based on idealized stratification profiles, that this effect may indeed be significant in equatorial seas [11,12]. However, profiles in the Atlantic do not appear likely to yield harmonic generation due to relatively weaker and more shallow pycnoclines. The remainder of this paper is organized as follows. The weakly nonlinear theory for harmonic generation is reviewed in Sec. II, followed by a description of the ARGO ocean stratification profile data in Sec. III and the method used to calculate the harmonic mode characteristics from these profiles in Sec. IV. The results of the harmonic mode calculations using those profiles are presented in Sec. V and interpreted in terms of the weakly nonlinear theory in Sec. VI.

II. WEAKLY NONLINEAR THEORY

The weakly nonlinear theory outlined here summarizes relevant results from [11,12]. Using the previously developed theoretical framework for an inviscid Boussinesq fluid on an f-plane with buoyancy frequency $N(z)$ and rotation frequency f, the weakly nonlinear solution is constructed in terms of the stream function $\psi(x, z, t)$, with $u \equiv \partial_z \psi$ and $w \equiv -\partial_x \psi$. The governing equations are [18]

$$\partial_t^2 \nabla^2 \psi + N^2 \partial_x^2 \psi + f^2 \partial_z^2 \psi = -\partial_t J(\nabla^2 \psi, \psi) - \frac{g}{\rho_o} \partial_x J(\rho, \psi) - f \partial_z J(v, \psi), \qquad (1)$$

$$\partial_t \rho + J(\rho, \psi) + \frac{\rho}{g} N^2 \partial_x \psi = 0, \qquad (2)$$

$$\partial_t v + J(v, \psi) + f \partial_z \psi = 0, \qquad (3)$$

where $\nabla^2 \equiv \partial_x^2 + \partial_z^2$, and the Jacobian is $J(a, b) \equiv (\partial_x a)(\partial_z b) - (\partial_x b)(\partial_z a)$. The mean fluid density is ρ_o, and ρ is the density perturbation from the mean stratification due to the internal wave motion.

Gravity is aligned with the vertical (z) axis. Viscosity and diffusion are neglected. If the Jacobian terms are neglected, these equations reduce to the standard linear internal wave equations.

Following the approach of [11], the solution is decomposed into a linear "parent mode" solution ψ_o with frequency ω and horizontal wave number k, and a (smaller amplitude) harmonic perturbation $\delta\psi$, as

$$\psi(x, z, t) = [a_o\psi_o(z)e^{i(kx-\omega t)} + \text{c.c.}] + \delta\psi(x, z, t), \tag{4}$$

where ψ and $\delta\psi$ are real, ψ_o is complex, and c.c. denotes complex conjugate. The constant a_o gives the amplitude of the parent mode, while ψ_o is a normalized solution of the linear internal wave equation. The density perturbation ρ and horizontal (meridional) velocity component v are similarly decomposed. Inserting Eq. (4) into Eq. (1), the parent mode obeys the standard linear equation:

$$\partial_z^2\psi_o + k^2\frac{N^2 - \omega^2}{\omega^2 - f^2}\psi_o = 0. \tag{5}$$

As shown in [11], the harmonic perturbation $\delta\psi$ obeys

$$\partial_t^2\nabla^2\delta\psi + N^2\partial_x^2\delta\psi + f^2\partial_z^2\delta\psi = -\frac{k^3}{\omega}\frac{(2\omega)^2 - f^2}{\omega^2 - f^2}(\partial_z N^2)[a_o^2\psi_o^2 e^{2i(kx-\omega t)} + \text{c.c.}] \tag{6}$$

to lowest order in ψ_o. Only the harmonic part of the forcing derived in [11] has been retained on the right-hand side of Eq. (6); the mean-flow part of the solution is not considered here. In uniform stratification ($\partial_z N^2 = 0$), there is no harmonic forcing for $\delta\psi$. Equation (6) shows that any internal wave propagating in vertically varying stratification (non-zero $\partial_z N^2$), such as an ocean environment with a pycnocline, generates harmonics. These may be bound harmonics of the incident wave or freely propagating waves. Mathematically, Eq. (6) is analogous to a system of forced simple harmonic oscillators with forcing frequency 2ω and wave number $2k$.

The steady-state, forced (or bound) harmonic solution of Eq. (6) is found by substituting $\delta\psi = \delta\psi_s(z)\exp[2i(kx - \omega t)] + \text{c.c.}$ for a double-frequency (2ω), double-wave-number ($2k$) harmonic into Eq. (6), as shown in [11]:

$$\partial_z^2\delta\psi_s + (2k)^2\frac{N^2 - (2\omega)^2}{(2\omega)^2 - f^2}\delta\psi_s = \frac{k^3}{\omega}\frac{\partial_z N^2}{(\omega^2 - f^2)}a_o^2\psi_o^2. \tag{7}$$

This equation is the generalization of the steady-state harmonic solution of [5] for a rotating fluid (nonzero f). Note the structure of the left-hand side of Eq. (7) mimics that of the linear equation for ψ_o Eq. (5). If the harmonic forcing frequency (2ω) and wave number ($2k$) are sufficiently close to those of a freely propagating solution of Eq. (5), resonance occurs (like a forced harmonic oscillator) and the harmonic mode amplitude is significant. Such conditions are a special case of triadic resonances in nonuniform stratifications [8], with the parent wave ψ_o comprising two components of the triad and the harmonic wave $\delta\psi_s$ being the third. An analytic solution for the steady-state harmonic was found for a three-layer fluid in [11].

Baker and Sutherland [12] showed that for a low-mode parent wave in near-resonant conditions, the harmonic mode amplitude will undergo a slow oscillation on a timescale much longer than ω^{-1}. This is represented mathematically by allowing the harmonic amplitude to vary slowly in time. By assuming a separation of timescales [12], constructed solutions for the harmonic using orthogonal basis functions are defined here as

$$\delta\psi \equiv e^{2i(kx-\omega t)}\sum_j a_j(t)\psi_j(2k, z) + \text{c.c.}, \tag{8}$$

where (k, ω) are the wave number and frequency of the parent mode, and a_j is the amplitude of the dimensionless orthonormal basis functions $\psi_j(k)$. Here the index j denotes the jth mode of the linear solution for the horizontal wave number k:

$$\partial_z^2 \psi_j + k^2 \frac{N^2 - \omega_j^2}{\omega_j^2 - f^2} \psi_j = 0, \tag{9}$$

$$\int_{-H}^{0} \psi_i \psi_j (N^2 - f^2) dz = \delta_{ij} H \omega_j^2. \tag{10}$$

Here $\omega_j(k)$ is the frequency of mode j with horizontal wave number k, and H is the depth of the water column. By definition, the parent mode frequency is $\omega = \omega_1(k)$ for a mode-1 parent wave. Following [12], substituting Eq. (8) into Eq. (6), utilizing the orthonormality of the basis functions Eq. (10), and neglecting the second time derivative of a_j (assumed small) yields

$$\frac{da_j}{dt} - i\epsilon_j \omega a_j = -i a_o^2 M_j, \tag{11}$$

$$\epsilon_j \equiv \frac{(2\omega)^2 - \omega_j^2(2k)}{(2\omega)^2}, \tag{12}$$

$$M_j \equiv \frac{k}{H\omega_j^2(2k)} \frac{(2\omega)^2 - f^2}{4(\omega^2 - f^2)} \frac{\omega_j^2(2k) - f^2}{4\omega^2} \int_{-H}^{0} \psi_o^2(k) \psi_j(2k) \partial_z N^2 dz, \tag{13}$$

where it is assumed, as in [12], that a_j grows slowly compared to the oscillation timescale $1/\omega$. Note that the first mode with wave number k is just the parent mode [$\psi_o \equiv \psi_1(k)$] with frequency ω, and that the stream functions ψ_j must be normalized as in Eq. (10). For realistic stratification profiles, it was found in [12] that the value of the dimensionless integral equivalent to Eq. (13) ($M_1 H/k$ in the present notation) is typically of order unity, and similar values were found for the ARGO data considered here (not shown). Assuming a pure parent mode as the initial condition [$a_j(t = 0) = 0$ for $j \neq 0$], the growth of the harmonic perturbation amplitudes can be calculated. The solution takes the form

$$a_j(t) = \frac{a_o^2 M_j}{\omega \epsilon_j}(1 - e^{i\epsilon_j \omega t}). \tag{14}$$

Here j is the index (mode number) of the wave-number $2k$ mode with frequency closest to 2ω, yielding the smallest value of ϵ_j. The harmonic mode amplitude scales as $1/\epsilon_j$, and its amplitude oscillates slowly with frequency $\epsilon_j \omega$. From Eq. (14), the ratio of the magnitude of the (oscillatory) harmonic mode to the parent mode amplitude is $a_o M_j/\omega \epsilon_j$. Note that although the slowly varying amplitude theory also permits a steady solution [12], it differs from the steady-state bound harmonic solution of [11]. Hence both approaches are used here to provide independent estimates of the possible harmonic effect.

III. OCEANIC STRATIFICATION DATA

This analysis uses approximately 390 000 ARGO stratification profiles collected during the period from 2009 to 2017 and retrieved online from [17]. The present analysis is limited to latitudes less than 60 degrees, since rotation is expected to inhibit the harmonic effect at latitudes exceeding ~10–20 degrees [11,12]. Each ARGO data profile typically extends to between 40% and 60% of the full ocean depth. Most profiles include a well-defined pycnocline within the measured portion of the water column, which is the most significant segment of the water column for this analysis, since the largest gradients of N typically occur there. In order to produce a complete stratification profile for stream-function calculations, values of N in the unmeasured part of the water column are estimated by taking the deepest 5% of the measured values and assigning their mean value to the
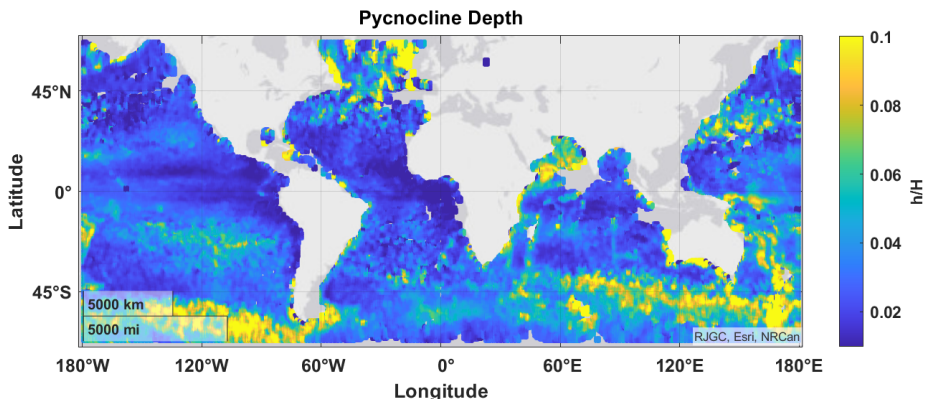
FIG. 1. The mean value of the dimensionless depth of the pycnocline base, h/H, of the ARGO profiles at each location.

unmeasured portion of the water column (i.e., constant buoyancy frequency). This extrapolation method is chosen to avoid adding any nonzero gradients to the water column, since nonzero values of $\partial_z N$ drive the harmonic generation mechanism. Results were not found to be sensitive to variations in the method for assigning the deep ocean stratification value in a number of test cases.

Given that the weakly nonlinear interaction is associated with gradients in N^2, the characteristics of the pycnocline are of primary relevance to the present analysis. The pycnocline is defined here as the region of increased N in the vicinity of the maximum value of N, denoted N_m, in the measured profile. To formulate a quantitative definition, the pycnocline stratification is compared to the buoyancy frequency in the deep ocean, defined here as the mean of the values in the lower two-thirds of the water column. This threshold was selected because nearly all ARGO profiles include measurements to at least this depth. Hence the deep buoyancy frequency, denoted N_o, is computed using a portion of the water column that includes both measured and extrapolated values of N. The value of N_o is typically between 0 and 2 cph. Comparing this to the maximum buoyancy frequency N_m, the pycnocline is defined here as the range of depths around the maximum for which N^2 is greater than a threshold value given by $(N_m^2 + 2N_o^2)/3$. In other words, the density gradient in the pycnocline exceeds the deep ocean mean density gradient by at least $1/3$ of the difference between the maximum and deep ocean values of N^2. The depths at which N^2 first crosses this threshold value above and below the depth of the maximum define the top and bottom of the pycnocline. These depths nominally correspond to the depths $-h + \delta$ and $-h$ in the three-layer idealized model of [11]. Finally, the density change $\Delta\rho$ across the pycnocline is computed by integrating N^2 between the two bounding depths and applying the definition of N^2 (proportional to the density gradient). Note that these definitions of pycnocline characteristics are not used for the calculations of the nonlinear harmonic effect; they are for interpretative purposes only.

Figure 1 presents a global map of the mean depth of the base of the pycnocline h relative to the water depth H as computed from the measured profiles by the method described above. The map was produced by spatially binning the profiles into 0.2-degree by 0.2-degree boxes in latitude and longitude, and averaging the pycnocline depth h for each profile within the box. In most locations, the dimensionless pycnocline depth h/H was less than 0.1. In equatorial regions (here defined as latitudes less than 15 degrees) it was usually less than 0.05, with the shallowest pycnoclines found in the Atlantic and Eastern Pacific. The deepest pycnoclines were generally found in the Southern Ocean and in the North Atlantic. These observations are generally consistent with other studies of the upper ocean pycnocline characteristics [19]. The pycnocline buoyancy change $g\Delta\rho/\rho_o$, normalized by $H(N_o^2 - \omega^2)$, is presented in Fig. 2 on a logarithmic (base-10) color scale. The reason for this specific normalization will be made clear in Sec. VI. In the equatorial waters of the Pacific
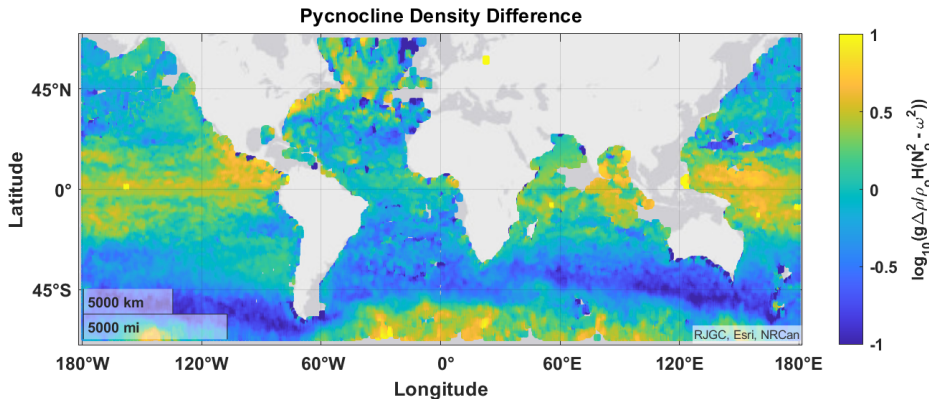
FIG. 2. The mean value of the dimensionless density change $g\Delta\rho/[\rho_o H(N_o^2 - \omega^2)]$ across the pycnocline computed from ARGO data.

and Indian Oceans, this normalized density change is often $\sim$3 or more. It is $\sim$1 or less in most of the Atlantic, and also at mid-latitudes. Larger values also appear in the North Atlantic and Southern Ocean.

IV. NUMERICAL CALCULATION OF MODES

The values of buoyancy frequency from each individual ARGO vertical profile (including the extrapolation to the sea floor) are used to form the basis of the numerical grid for calculating the internal wave modes. To improve the conditioning of the matrix inversion needed for this calculation, linear interpolation is used to fill in three additional data points, spaced evenly between each measured data point (*i.e.,* depth z_j), producing a discrete set of buoyancy frequency values N_j at depths z_j. Because the ARGO profiles do not extend to the sea floor, the lower part of the water column is gridded with the same vertical resolution as the measured ARGO data and assigned the deep ocean buoyancy frequency N_o as described in the previous section. The resulting discretized profile of N values typically had $\sim$2000 data points, with a spatial resolution of a few meters in depth.

For a measured oceanic profile, the parent mode is calculated by discretizing Eq. (5) using a Taylor expansion to second order, using the stratification profile N_j generated from the measured data as described above. The frequency of the semidiurnal ($\sim$12-hour period) internal tide ($\omega \simeq 1.4 \times 10^{-4}$ s^{-1}) is used, and the horizontal wave number k and lowest mode ψ_o are calculated numerically using MATLAB's matrix eigenfunction solver. Because harmonic generation is a nonlinear effect, it depends on the parent mode amplitude a_o. Here, a_o for each profile is set by choosing a representative value for the maximum horizontal current, defined as $U_o = \max(|a_o\partial_z\psi_o|)$, of 1 cm/s. For almost all profiles, the maximum horizontal current occurs at the sea surface. This choice is motivated by the typical amplitude of currents associated with internal tides being on the order of centimeters per second [16], making the choice of 1 cm/s a conservative value. The expected harmonic response to a parent mode with a maximum horizontal current greater than 1 cm/s would increase with the square of the current. Although the amplitudes of oceanic internal tides vary, the use of a constant amplitude a_o here focuses attention on the potential for harmonic generation due to geographic changes in ocean stratification, without introducing additional variations associated with differing parent mode amplitudes.

Given the parent mode solution ψ_o and wave number k, the steady-state harmonic mode $\delta\psi_s$ is computed by discretizing Eq. (7) on the same grid used for the parent mode and performing matrix inversion to solve for $\delta\psi_s$. To evaluate the resonance parameter ϵ [Eq. (12)] and the unsteady theory of [12], the modes and frequencies for wave number $2k$ are computed numerically from Eq. (9) by
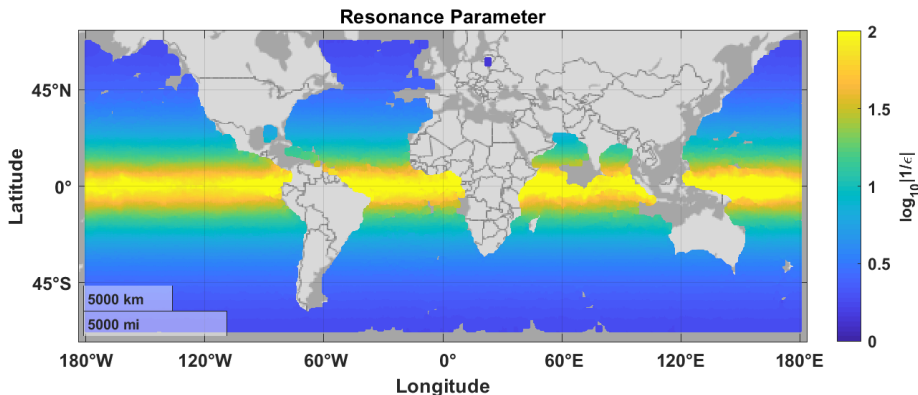
FIG. 3. Global map of the mean value of the resonance parameter $1/\epsilon$ (logarithmic color scale). The smallest values of $|\epsilon|$ (yellow) are found near the equator.

again using the MATLAB matrix eigenfunction solver. Given these modes, the harmonic response $a_o M_1/\omega\epsilon$ for the unsteady theory of [12] is computed using Eq. (13).

V. RESULTS

Using the numerically calculated parent mode horizontal wave number k for each profile, the harmonic frequency $\omega_1(2k)$ corresponding to wave number $2k$ is determined and the mode-1 resonance parameter ϵ [Eq. (12)] from [12] is computed. The values of ϵ from each individual profile are spatially binned into 0.2 degree boxes (as with the stratification profile parameters in Figs. 1 and 2) and are presented in Fig. 3. The color scale shows $1/\epsilon$ and is logarithmic (base 10), with yellow indicating values of ϵ smaller than 0.01. It is clear that ϵ depends almost solely on latitude, with the resonance parameter moving away from zero with increasing latitude (rotation) for the ARGO profiles. Within a few degrees of the equator, values of ϵ are typically between 0.01 and 0.05, indicating near resonance between the mode-1 semidiurnal internal tide and its first harmonic. It increases to ∼0.1 at latitudes of ∼30 degrees and approaches ∼1 at ∼60 degrees. The work of [12] indicates that $\epsilon \ll 1$ is a necessary condition for strong harmonic generation, and Fig. 3 shows that this condition holds in equatorial waters globally.

Using the results from weakly nonlinear theory in Sec. II, two measures of the potential harmonic effect are calculated from the parent mode stream functions for the representative horizontal current value U_o of 1 cm/s described above. For the steady-state bound harmonic amplitude $\delta\psi_s$ [Eq. (7)] from [11], Fig. 4 presents results for the integrated amplitude ratio R, defined by [12] as

$$R^2 \equiv \frac{\int_{-H}^{0} |\delta\psi_s|^2 dz}{\int_{-H}^{0} |a_o\psi_o|^2 dz}. \tag{15}$$

Note that R^2 can be interpreted as a ratio of kinetic energy in the harmonic mode to that of the parent mode. Since the vertical velocity is given by the wave number multiplied by the stream function, $4R^2$ corresponds to the ratio of the total kinetic energy in the vertical component of velocity of the harmonic to that of the parent mode. Mean values of R, computed from the measured ARGO profiles and geographically binned as in Fig. 3, are shown in Fig. 4. Unlike the resonance parameter ϵ, the actual harmonic response is not solely determined by latitude. A value of R greater than 0.1 indicates that the steady-state harmonic integrated amplitude exceeds 10% of the parent wave integrated amplitude for the assumed current of $U_o = 1$ cm/s. This indicates potential for a harmonic response to exceed the limitations of weakly nonlinear theory and possibly produce a more strongly nonlinear wave. For larger values of U_o, the value of R would be proportionally larger. (For example,
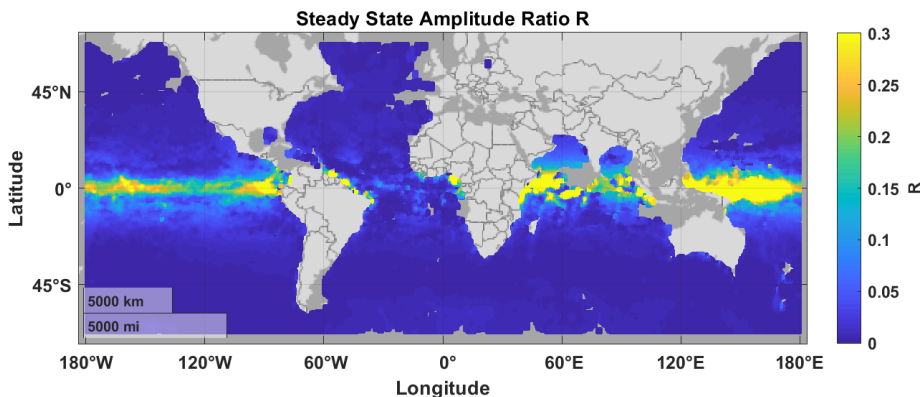
FIG. 4. The mean value of the ratio R of the steady-state forced harmonic magnitude to the parent mode magnitude. The largest amplitudes (yellow) are generally found in the equatorial waters of the Pacific and Indian Oceans.

if $R = 0.1$ for $U_o = 1$ cm/s, the corresponding value for $U_o = 5$ cm/s would be $R = 0.5$.) While values of R greater than 0.1 are only found near the equator, R remains small in the equatorial Atlantic, despite near resonance (small ϵ). If $\epsilon \ll 1$ were a sufficient condition for strong harmonic generation, all equatorial waters would exhibit the effect, but Fig. 4 indicates that this is not the case.

An alternate measure of the steady-state bound harmonic amplitude is the maximum horizontal current associated with the harmonic mode, given by $U_h = \max(|\partial_z \delta \psi|)$. The mean ratio of harmonic to parent current U_h/U_o was also computed, and the results closely mirrored those of Fig. 4 for R. For the measured ARGO profiles, the computed values of R and U_h/U_o never differed by more than a few percent.

For the unsteady harmonic amplitude theory of [12], Eq. (14) describes the evolution of the harmonic mode. The harmonic amplitude is given by $a_o M_1/\omega \epsilon$, where M_1 is given by Eq. (13). This ratio is presented in Fig. 5 for the assumed value of a_o corresponding to $U_o = 1$ cm/s. These results qualitatively match Fig. 4, but this method predicts a somewhat larger harmonic amplitude (typically by a factor of up to 2, depending on the individual profile) than the steady-state bound harmonic theory. The qualitative similarity of the results from the two different approaches adds
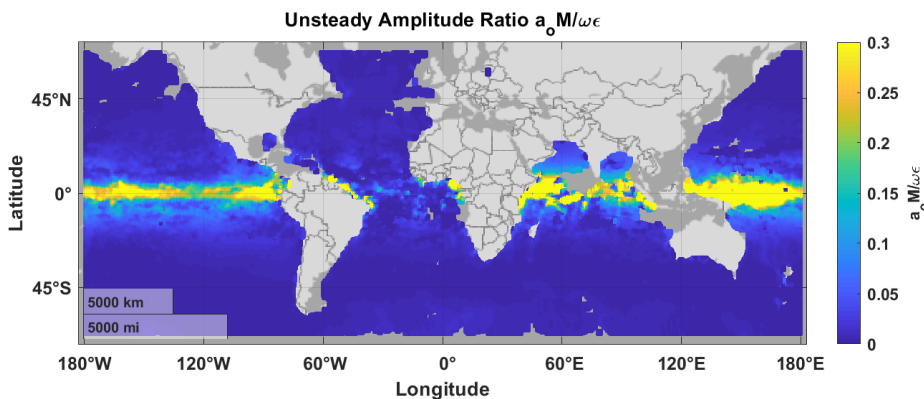

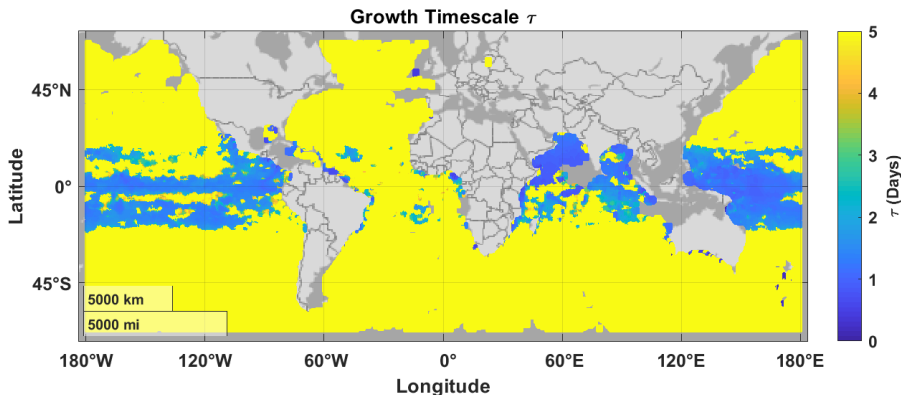FIG. 5. The mean value of the ratio $a_o M/\omega \epsilon$ from the unsteady theory of Ref. [12].

FIG. 6. The median time τ for the harmonic mode to reach an amplitude of $0.05a_o$ in the unsteady theory of Ref. [12].

confidence to the observation that strong harmonics may occur only near the equator but are not expected in the Atlantic.

The timescale for a harmonic to grow to significant amplitude can be estimated from the unsteady theory of [12] using Eq. (14). The time τ to grow to an amplitude of 5% of the parent mode ($0.05a_o$) is given by

$$\cos\left(\epsilon\omega\tau\right) = 1 - \frac{1}{2}\left(\frac{0.05\omega\epsilon}{a_o M}\right)^2. \tag{16}$$

This timescale is presented in Fig. 6 using the same geographic binning as the previous results. The color scale shows the median of the values of τ in days for the profiles in each geographic bin. The median of the data is used rather than the mean here, because some profiles have harmonic amplitudes less than $0.05a_o$, implying a τ of infinity. The typical timescale is a few days in the equatorial Pacific and Indian Oceans, consistent with the estimates of [12] for idealized profiles in near-resonance conditions.

The absence of a significant harmonic amplitude computed (by either of the measures presented) from the ARGO profiles in the equatorial Atlantic is an unexpected result of this analysis, given the similar values of ϵ (Fig. 3) across all equatorial oceans. This indicates that near resonance alone is not sufficient to generate a nonlinear harmonic mode. A possible theoretical explanation for this difference is presented in the next section.

VI. INTERPRETATION USING WEAKLY NONLINEAR THEORY

The absence of nonlinear harmonics in the equatorial Atlantic, despite near resonance with the semidiurnal internal tide, can be understood in terms of weakly nonlinear theory. A key difference between the Atlantic and the other oceans is the relative weakness of the density jump at the pycnocline, as seen in Fig. 2. This likely implies smaller buoyancy frequency gradients $\partial_z N^2$ and hence weaker harmonic forcing due to the appearance of this factor in Eqs. (7) (steady state) and (13) (slowly varying amplitude). However, the weakly nonlinear theory below suggests this may not be the only effect. The amplitude of the parent mode ψ_o^2 also appears in these equations, and the magnitude of this factor at the pycnocline (where $\partial_z N^2$ is largest) may also contribute to the difference in the estimated harmonic effect between the Atlantic and the other ocean basins. The significance of these effects is explored below using an idealized theory.

To illustrate the impact of the pycnocline characteristics on the parent mode, the three-layer piecewise linear solution of [11] is reduced to a two-layer solution using the limit method of [20]. The stratification is N_o below the pycnocline ($z < -h$) and zero above it. The pycnocline is
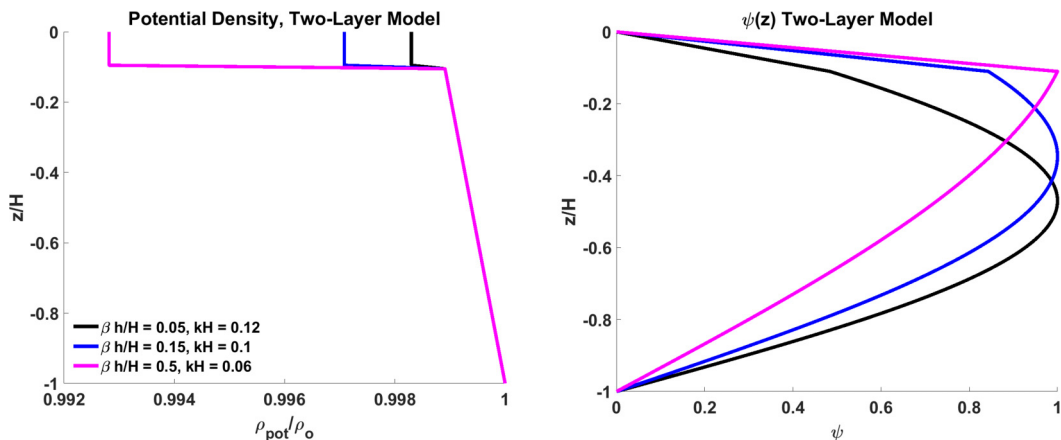
FIG. 7. Example parent mode solutions (right) for a two-layer stratification profile (left) with three different values of the dimensionless pycnocline density jump parameter β [Eq. (18)].

represented by a density jump $\Delta\rho$ at $z = -h$. The parameters h and $\Delta\rho$ in this model are intended to be analogous to the quantities shown in Figs. 1 and 2. The parent mode ψ_o is given by

$$\psi_o = a_o \begin{cases} -\frac{\sin q(H-h)}{\sinh q_m h} \sinh q_m z & -h < z < 0 \\ \sin[q(H+z)] & -H < z < -h \end{cases}$$

$$q^2 = k^2 \frac{N_o^2 - \omega^2}{\omega^2 - f^2}$$

$$q_m^2 = k^2 \frac{\omega^2}{\omega^2 - f^2}, \tag{17}$$

and the dispersion relation is

$$\tan q(H-h) = -\frac{q \tanh q_m h}{q_m - \beta q^2 H \tanh q_m h}$$

$$\beta \equiv \frac{g\Delta\rho}{\rho_o H (N_o^2 - \omega^2)}. \tag{18}$$

Here β is the dimensionless density jump across the pycnocline plotted in Fig. 2. This solution is equivalent to the result in [11] in the limit of a thin pycnocline and reduces to the result in [9] in the absence of rotation ($f = 0$).

The two-layer solution for ψ_o is presented in the right panel of Fig. 7 using three different values of β with a pycnocline depth of $h = 0.1H$ and deep stratification $N_o = 2$ cph. Corresponding potential density profiles ρ_{pot}/ρ_o (defined from the stratification profile using $N^2 = -\frac{g}{\rho_o}\frac{d\rho_{pot}}{dz}$) are shown in the left panel, illustrating the increase in pycnocline stratification with β. As $\beta h/H$ increases from 0.05 to 0.5, the maximum of ψ_o transitions from the center of the water column ($z \sim -H/2$) to the pycnocline $z \sim -h$ and the wave number kH decreases from 0.12 to 0.06. Hence the pycnocline parameter β divides the mode-1 parent solutions into two qualitatively different types. The first type occurs for a weak and shallow pycnocline (small β and $h \ll H$). In this case, the right-hand side of the dispersion relation [Eq. (18)] is approximately zero, and the dispersion relation yields $qH \simeq \pi$ for mode 1. In this case, the maximum value of ψ_o occurs near the middle of the water column, at $z \sim -H/2$. The black curve in Fig. 7 is an example of this type of solution.
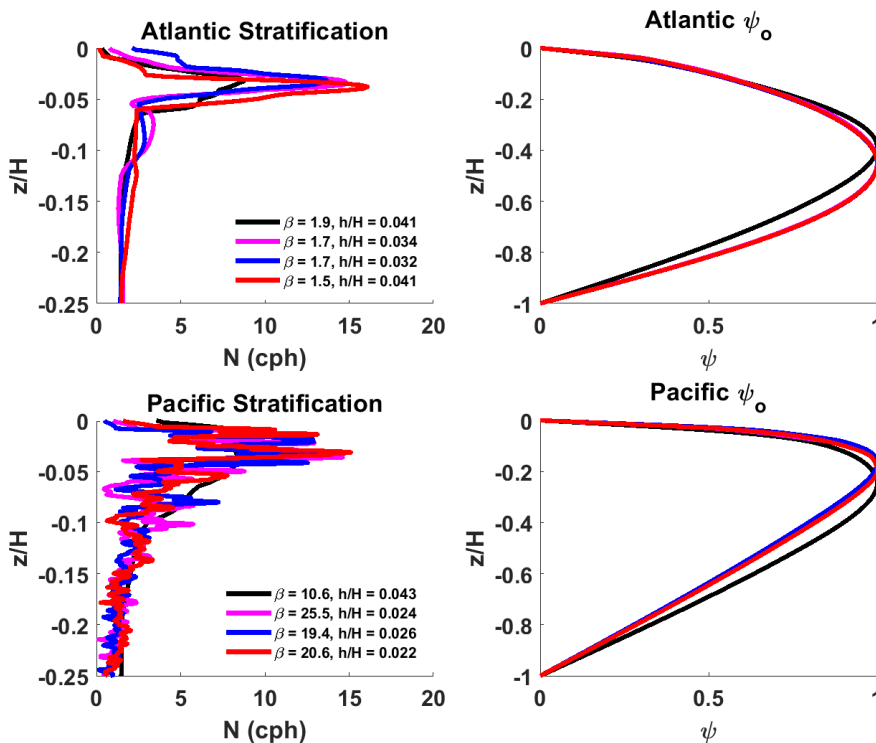
FIG. 8. Example Argo measured density profiles (left) and corresponding parent mode solutions (right) from several locations in the equatorial Atlantic (top) and Pacific (bottom). The pycnocline density jump parameter β [Eq. (18)] and depth h/H are indicated for each profile.

The amplitude of ψ_o at the pycnocline is small (compared to its maximum), yielding a relatively weak forcing of the harmonic mode.

In the second type of parent mode solution, the dispersion relation is more substantially altered by the presence of the pycnocline. In this case, β is large enough to cause the denominator of Eq. (18) to approach zero:

$$\beta q^2 H \tanh q_m h \sim q_m. \tag{19}$$

For solutions of this type, a wave number of $qH \sim \pi/2$ is required to find a solution to Eq. (18). This moves the maximum value of ψ_o toward the pycnocline depth $z \sim -h$. This is seen in Fig. 7 for $\beta h/H = 0.5$ (magenta curve). Assuming $q_m h << 1$ and $qH \sim \pi/2$, the pycnocline density jump [Eq. (19)], which yields the transition between ψ_o peaking near the middle of the water column ($z \sim -H/2$) and peaking near the pycnocline, can be expressed as

$$\frac{\beta h}{H} \sim \frac{4}{\pi^2}. \tag{20}$$

Equation (20) roughly separates the two qualitatively distinct types of mode-1 parent solutions. The change in the shape of ψ_o seen in Fig. 7 occurs between $\beta h/H \sim 0.1$ and $\beta h/H \sim 0.5$, consistent with the rough estimate of Eq. (20). This shift in the peak of ψ_o toward the pycnocline results in stronger harmonic forcing, since ψ_o is larger in amplitude at the pycnocline depth where the gradients of N^2 are found. The transition occurs gradually for $\beta h/H$ in the range of 0.1–0.5, and for realistic ocean stratifications may depend on the details of the profile $N(z)$.

Several example ARGO stratification profiles $N(z)$ are presented in Fig. 8 (only the upper quarter of the water column is shown), along with the corresponding stream functions ψ_o calculated
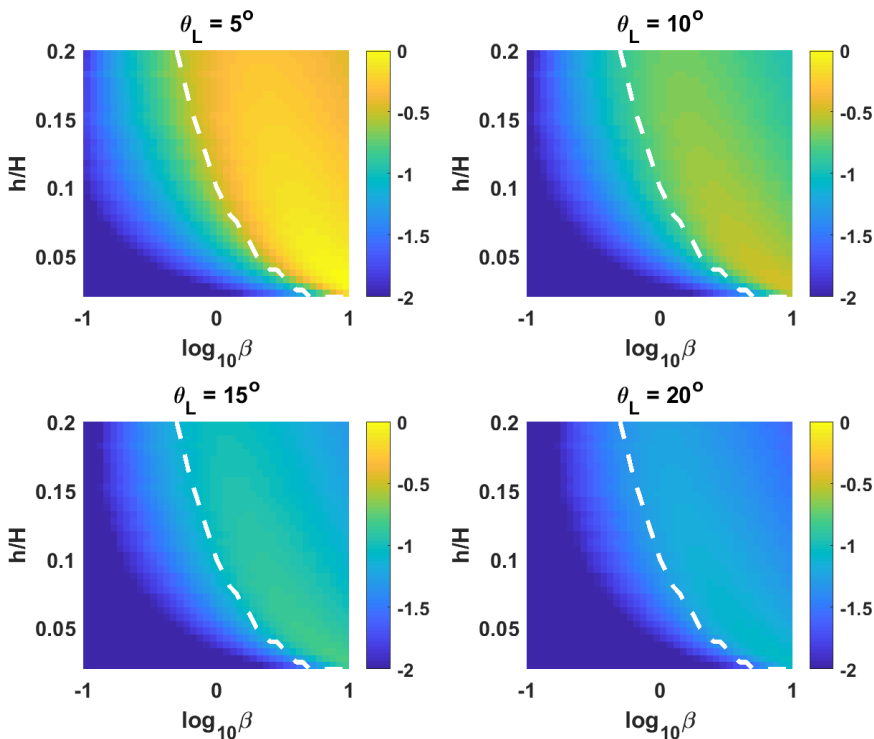
FIG. 9. Dependence of the harmonic amplitude ratio R on the dimensionless pycnocline depth h/H and density jump β for four latitudes θ_L in the two-layer stratification profile. The color scale is logarithmic (base 10). The dashed white line is $\beta h/H = 0.15$.

numerically from each profile. The profiles were drawn from data collected in the Atlantic (top) and Pacific (bottom) with latitudes of 10 degrees or less. Matching colors indicate which stream function was calculated from which profile. The values of β and h/H are given in the legend, and the profiles were selected to be among the larger values of $\beta h/H$ for each ocean basin. The Atlantic profiles shown have $\beta h/H$ between 0.05 and 0.1, and stream functions which peak near the middle of the water column ($z \sim -0.5H$). The Pacific profiles shown have $\beta h/H \sim 0.5$, and stream functions which peak closer to the pycnocline ($z \sim -0.2H$). Although the ARGO profiles have more structure than the simple two-layer model, the distinction between stream functions which peak near the center of the water column and those which peak near the pycnocline, and the significance of $\beta h/H$ as a governing parameter in this distinction, appears to apply to the ARGO data.

Stream functions with shallow maxima are generally found in the equatorial waters of the Pacific, but not the Atlantic. The more shallow maximum of ψ_o in the Pacific overlaps the depth band with gradients of N^2 and hence is expected to produce a stronger harmonic forcing. This is consistent with the stronger estimated harmonic response (Figs. 4 and 5) seen in the Pacific but not in the Atlantic. Note that the maximum of N has a similar value and occurs at a comparable dimensionless depth (a few percent of the water depth) in the examples shown for both oceans in Fig. 8. The shift in the stream function appears to be an important factor in the increased harmonic response.

Using the steady-state harmonic solution of [11], the theoretical harmonic mode amplitude ratio R is computed as a function of β. Although the solution of [11] uses a three-layer profile, a very thin pycnocline thickness was chosen here to approximate the two-layer case. The results for the harmonic amplitude ratio R for the chosen parent mode amplitude of $U_o = 1$ cm/s are presented in Fig. 9 as a function of pycnocline density parameter β and depth h/H. Results are shown for four
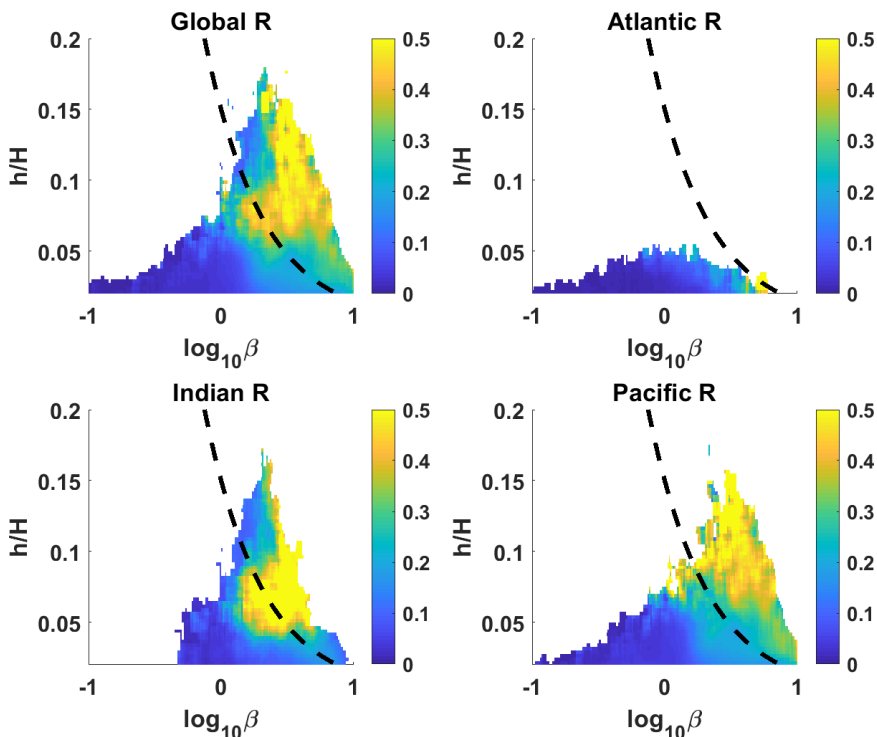
FIG. 10. The steady-state harmonic amplitude ratio R as a function of the dimensionless pycnocline depth h/H and density jump $\beta = g\Delta\rho/\rho_o(N_o^2 - \omega^2)H$ for latitudes less than 15 degrees using the full ARGO data set (upper left) and using three ocean basins individually. The dashed black line is $\beta h/H = 0.15$.

latitudes from 5 to 20 degrees. Results in the upper-left panel of Fig. 9 mimic those in Ref. [9] (Fig. 3 therein) in which rotation was neglected. They also correspond to those in Ref. [11] (Fig. 1 therein) for a finite-thickness pycnocline. The dashed white line corresponds to $\beta h/H \sim 0.15$, similar to the transition value suggested by Fig. 7 and Eq. (20). The largest amplitude ratios are found to the right of the white dashed line at all latitudes. Figure 9 demonstrates that in weakly nonlinear theory for a two-layer profile, steady-state harmonics of amplitude greater than 10% of the parent amplitude (for this ocean-inspired choice of a_o) occur only at low latitudes (where near resonance occurs) and only when $\beta h/H$ exceeds a value on the order of ~ 0.1.

The steady-state harmonic amplitude ratio R and the unsteady amplitude $a_o M/\omega\epsilon$ are computed from the ARGO data (Figs. 4 and 5) as a function of β and h/H. The results are presented in Figs. 10 and 11, respectively, in a manner analogous to Fig. 9. Here, all profiles from latitudes below 15 degrees were included, and the stratification profile parameters h/H and β for each profile were computed as described in Sec. III above. The upper-left panel of each figure presents the data for all oceans, while the three remaining panels present data from the Atlantic, Indian, and Pacific ocean basins separately. A transition value of $\beta h/H = 0.15$ is indicated by the black dashed lines, as in Fig. 9. As with the two-layer analytic solution (Fig. 9), both steady-state and unsteady harmonic amplitudes exceeding 20% of the parent amplitude (green/yellow on the plots) are mostly found in profiles with β exceeding this value. Comparing the three ocean basins, the Atlantic lacks the combination of deeper pycnoclines ($h/H > 0.05$) and larger density changes ($\beta h/H > 0.15$) found elsewhere. The value of β needed for a stronger harmonic is larger for shallow pycnoclines, and only a small fraction of the Atlantic profiles exceed this value. In contrast, deeper pycnoclines with β exceeding the transition value are more common in the Pacific and Indian basins, accounting for the higher likelihood of a stronger harmonic response calculated there.
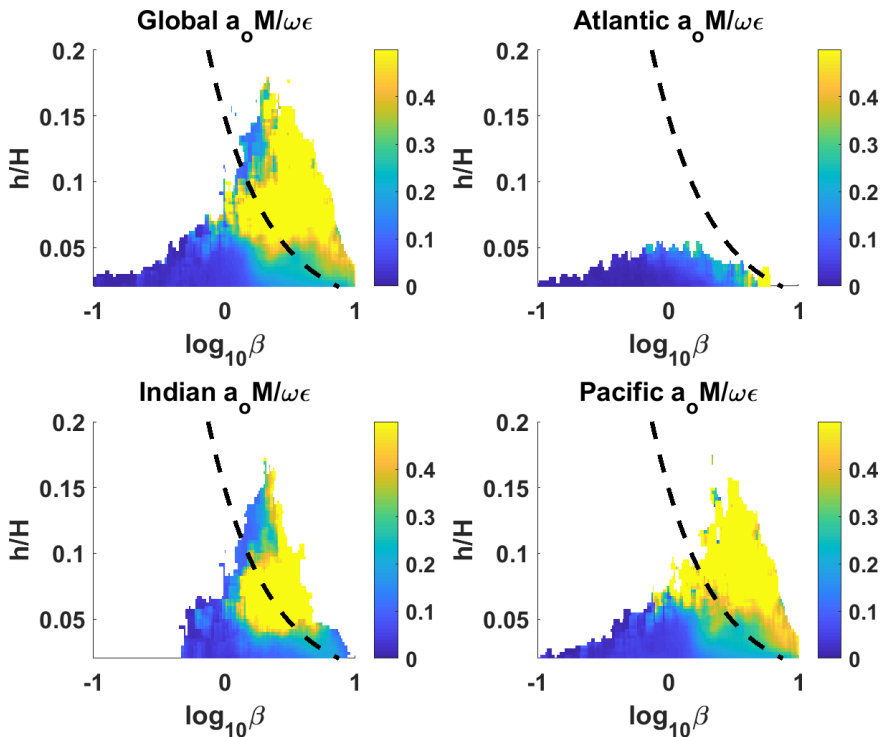
FIG. 11. The ratio $a_o M/\omega\epsilon$ from the unsteady theory of [12] as a function of the dimensionless pycnocline depth h/H and density jump $\beta = g\Delta\rho/\rho_o(N_o^2 - \omega^2)H$ for latitudes less than 15 degrees using the full ARGO data set (upper left) and using three ocean basins individually. The dashed black line is $\beta h/H = 0.15$.

VII. DISCUSSION

In this work, ARGO data are analyzed to estimate the theoretical potential for mode-1 semidiurnal internal tides to form nonlinear harmonics. The possibility of a significant (exceeding $\sim 10\%$ of parent mode amplitude) response is found near the equator, except in the Atlantic. As previously suggested [12], near resonance between the frequency of the lowest mode with wave number $2k$ and double the frequency of the lowest mode with wave number k appears to be a necessary condition for a harmonic response. This condition, defined by $\epsilon \ll 0.1$ [Eq. (12)], is met globally for latitudes below ~ 15 degrees. However, a secondary condition of a sufficiently deep and strong pycnocline, parameterized by the condition $\beta h/H > \sim 0.1$–0.5 for the dimensionless pycnocline density change β [Eq. (18)] is also found to be necessary for a harmonic response. This secondary condition is rarely met by the ARGO profiles in the equatorial Atlantic but is regularly met in other ocean basins.

Harmonics of the semidiurnal internal tides have been observed in the South China Sea by [14], although the generating mechanism for these data is not known. Unfortunately, ARGO data in the South China Sea corresponding to these observations were not available for this study. Analysis of MOODS [15] profiles by [9] yielded $h/H \sim 0.03$ and $\beta \sim 0.7$, which puts those observations somewhat below the estimated range of transition values ($\beta h/H \sim 0.02$). However, the parent mode amplitude in [14] is larger than the value of U_o used here (~ 10 cm/s, compared to 1 cm/s used here), which would favor a stronger harmonic response than indicated by Fig. 9. These profile parameter values appear to be consistent with the modest harmonic current amplitude (on the order of 10% of the parent mode current) observed by [14]. Again, consistency is not proof that the nonlinear harmonic generation mechanism considered here is the cause of the observed harmonics.

Future warming of the upper ocean mixed layer due to climate change will presumably increase the typical density difference across the pycnocline. Every degree increase in temperature in the

mixed layer increases $\Delta\rho/\rho_o$ by $\sim 2.4 \times 10^{-4}$ and the dimensionless parameter β by ~ 1, assuming $N_o \sim 0.5$ cph and $H \sim 3000$ m as typical ocean values. If the pycnocline depth is unchanged, the increasing gradients of N^2 at the pycnocline would favor a stronger harmonic response. This could make the internal tides propagating toward the equator more prone to nonlinear harmonic generation as the climate warms.

The theoretical approaches used here exclude many effects which are present as internal waves propagate across ocean basins, including horizontal variations in water depth, stratification, rotation, and the presence of horizontal currents. In future work, modifications of the theory would permit estimation of the importance of these effects. Investigation of the dynamics of energy exchange between parent and harmonic modes using ARGO profile data, such as was performed in [12] for idealized profiles, would also be worthwhile.

[1] S. Wunsch, and A. Brandt, Laboratory experiments on internal wave interactions with a pycnocline, Exp. Fluids **53**, 1663 (2012).

[2] M. J. Mercier, M. Mathur, L. Gostiaux, T. Gerkema, J. M. Magalhaes, J. C. B. da Silva, and T. Dauxois, Soliton generation by internal tidal beams impinging on a pycnocline: Laboratory experiments, J. Fluid Mech. **704**, 37 (2012).

[3] S. Wunsch, I. Delwiche, G. Frederick, and A. Brandt, Experimental study of nonlinear harmonic generation by internal waves incident on a pycnocline, Exp. Fluids **56**, 87 (2015).

[4] N. Grisouard, C. Staquet, and T. Gerkema, Generation of internal solitary waves in a pycnocline by an internal wave beam: A numerical study, J. Fluid Mech. **676**, 491 (2011).

[5] P. J. Diamesses, S. Wunsch, I. Delwiche, and M. P. Richter, Nonlinear generation of harmonics through the interaction of an internal wave beam with a model oceanic pycnocline, Dyn. Atmos. Oceans **66**, 110 (2014).

[6] S. Wunsch, H. Ku, I. Delwiche, and R. Awadallah, Simulations of nonlinear harmonic generation by an internal wave beam incident on a pycnocline, Nonlinear Processes Geophys. **21**, 855 (2014).

[7] S. A. Thorpe, Nonlinear reflection of internal waves at a density discontinuity at the base of a mixed layer, J. Phys. Oceanogr. **28**, 1853 (1998).

[8] D. Varma, and M. Mathur, Internal wave resonant triads in finite-depth non-uniform stratifications, J. Fluid Mech. **824**, 286 (2017).

[9] S. Wunsch, Nonlinear harmonic generation by diurnal tides, Dyn. Atmos. Oceans **71**, 91 (2015).

[10] B. R. Sutherland, Excitation of superharmonics by internal modes in a non-uniformly stratified fluid, J. Fluid Mech. **793**, 335 (2016).

[11] S. Wunsch, Harmonic generation by nonlinear self-interaction of a single internal wave mode, J. Fluid Mech. **828**, 630 (2017).

[12] L. E. Baker, and B. R. Sutherland, The evolution of superharmonics excited by internal tides in nonuniform stratification, J. Fluid Mech. **891**, R1 (2020).

[13] B. R. Sutherland, and M. S. Dhaliwal, The nonlinear evolution of internal tides. Part 1: The superharmonic cascade, J. Fluid Mech. **948**, A21 (2022).

[14] X. Xie, X. Shang, van H. Haren, and G. Chen, Observations of enhanced nonlinear instability in the surface reflection of internal tides, Geophys. Res. Lett. **40**, 1580 (2013).

[15] MOODS, https://www.ncei.noaa.gov/access/metadata/landing-page/bin/iso?id=gov.noaa.nodc:0049269.

[16] Z. Zhao, M. H. Alford, J. B. Girton, L. Rainville, and H. Simmons, Global observations of open-ocean mode-1 M$_2$ internal tides, J. Phys. Oceanogr. **46**, 1657 (2016).

[17] ARGO, https://argo.ucsd.edu/.

[18] P. H. LeBlond and L. A. Mysak, *Waves in the Ocean* (Elsevier, New York, 1981).

[19] G. Serazin, A. M. Treguier, and C. A. de Boyer Montegut, Seasonal climatology of the upper ocean pycnocline, Front. Mar. Sci. **10**, 1120112 (2023).

[20] S. Wunsch, Nonlinear harmonic generation by internal waves in a density staircase, Phys. Rev. Fluids **3**, 114803 (2018).